The Astrophysical Journal Letters, 750:L33 (5pp), 2012 May 10 doi:10.1088/2041-8205/750/2/L33

ON THE ORIGIN OF THE $1/f$ SPECTRUM IN THE SOLAR WIND MAGNETIC FIELD

Andrea Verdini[1], Roland Grappin[2,3], Rui Pinto[4], and Marco Velli[5]
[1] Solar-Terrestrial Center of Excellence-SIDC, Royal Observatory of Belgium, Bruxelles, Belgium; verdini@oma.be
[2] LUTH, Observatoire de Paris, CNRS, Université Paris-Diderot, 92190 Meudon, France; Roland.Grappin@obspm.fr
[3] LPP, Ecole Polytechnique, 91128 Palaiseau, France
[4] Laboratoire AIM Paris-Saclay, CEA/Irfu, and Université Paris-Diderot CNRS/INSU, Gis-sur-Yvette, France; rui.pinto@cea.fr
[5] Jet Propulsion Laboratory, California Institute of Technology, Pasadena, CA, USA; mvelli@jpl.nasa.gov
Received 2012 March 12; accepted 2012 March 29; published 2012 April 20

ABSTRACT

We present a mechanism for the formation of the low-frequency $1/f$ magnetic spectrum based on numerical solutions of a shell-reduced MHD model of the turbulent dynamics inside the sub-Alfvénic solar wind. We assign reasonably realistic profiles to the wind speed and the density along the radial direction, and a radial magnetic field. Alfvén waves of short periodicity (600 s) are injected at the base of the chromosphere, penetrate into the corona, and are partially reflected, thus triggering a turbulent cascade. The cascade is strong for the reflected wave while it is weak for the outward propagating waves. Reflection at the transition region recycles the strong turbulent spectrum into the outward weak spectrum, which is advected beyond the Alfvénic critical point without substantial evolution. There, the magnetic field has a perpendicular power-law spectrum with slope close to the Kolmogorov $-5/3$. The parallel spectrum is inherited from the frequency spectrum of large (perpendicular) eddies. The shape is a double power law with slopes of $\simeq -1$ and -2 at low and high frequencies, respectively, with the position of the break depending on the injected spectrum. We suggest that the double power-law spectrum measured by *Helios* at 0.3 AU, where the average magnetic field is not aligned with the radial (contrary to our assumptions), results from the combination of such different spectral slopes. At low frequency the parallel spectrum dominates with its characteristic $1/f$ shape, while at higher frequencies its steep spectral slope (-2) is masked by the more energetic perpendicular spectrum (slope $-5/3$).

Key words: magnetohydrodynamics (MHD) – plasmas – solar wind – turbulence

Online-only material: color figures

1. INTRODUCTION

At heliocentric distances of about 0.3 AU the magnetic field spectrum in the fast streams of the solar wind has a form of a double power law with a break at about $f = 5 \times 10^{-3}$ Hz and a slope of approximately -1 and $-5/3$ at lower and higher frequencies, respectively (Bavassano et al. 1982; Denskat & Neubauer 1983; Bruno & Carbone 2005). Fluctuations in these two ranges have a different evolution with distance (Bavassano et al. 1982; Marsch & Tu 1990; Roberts 1992). The low-frequency part approximately follows the WKB behavior, $E \propto r^{-3}$, dictated by the solar wind expansion. The high-frequency part instead decreases much sharply, its energy content being depleted by the turbulent cascade, and maintains approximately the same spectral slope. Therefore, the frequency break shifts to lower and lower frequency as the heliocentric distance increases, the $1/f$ spectrum occupying the range 3×10^{-6} Hz $\lesssim f \lesssim 8 \times 10^{-5}$ Hz at 1 AU (Matthaeus & Goldstein 1986). The energy in the low-frequency tail progressively contributes to the turbulent heating of the solar wind. The spectral evolution can be understood as a competition between the expansion time scale and the cascade time scale, regulating the decay of energy respectively at small and large scales (Tu et al. 1984), but the origin of the $1/f$ spectrum is still a matter of debate.

There are some indications that it may have a genuine solar origin, reflecting the emergence, cancellation, and sinking of the magnetic field at the photosphere: spectra built from magnetogram data at low-intermediate latitudes show a $1/f$ slope at low wavenumbers, which also correlate to the spectrum of density fluctuations in the heliosphere (Matthaeus et al. 2007). In this view, the formation mechanism relies on magnetic reconnection, occurring over a hierarchy of scales as a stochastic process with some self-similar properties. Reconnection, this time in the corona, has also been invoked as the underlying process, since the timescale associated with the restructuring of coronal magnetic field is about 1 day, i.e., in the range of observed frequencies (Close et al. 2004). Recently, the formation of a $1/f$ spectrum has been observed in homogeneous incompressible MHD simulations of very long duration, probably originating from an inverse cascade not associated with well-defined invariants (Dmitruk & Matthaeus 2007; Dmitruk et al. 2011). Other ideas rely on large-scale properties of the corona and solar wind: reflection was suggested as a possible mechanism to obtain a k^{-1} spectrum from an isotropic cascade of Alfvén waves coming from the Sun in the expanding solar wind (Velli et al. 1989). The linear evolution of Alfvénic pulses excited in the corona leads to a signal (outside the Alfvénic critical point) which has periodicities of about 15–30 minutes (ringing of the corona; Hollweg & Isenberg 2007). Though this period appears too low to account for the entire range of observed frequencies, as suggested by the authors, the ringing of the corona could play a role in the formation of the $1/f$ spectrum.

In this Letter, we combine the latter two ideas, the ringing of the corona and nonlinear interactions with reflected waves, to study the formation of the magnetic field spectrum advected by the solar wind. To this aim, we use a shell-reduced MHD model (Verdini et al. 2009) to follow the onset of turbulence resulting from the coupling between Alfvén waves propagating in the chromosphere, corona, and sub-Alfvénic solar wind. The solar wind profiles (Alfvén speed, velocity, and density profiles)

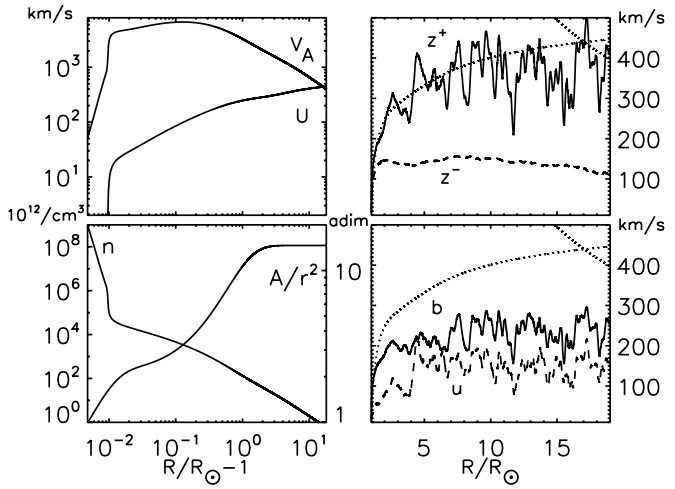

Figure 1. Left panels: solar wind model. Profiles of the Alfvén and wind speed (top) and of the density and overexpansion $\mathcal{F} = A(r)/r^2$ (bottom). Right panels: snapshots of the amplitude of the Elsässer variables (top) and of the velocity and magnetic fluctuations (bottom). The Alfvén and wind speed are also overplotted as dotted lines.

are given steady numerical solutions of the slow wind model by Pinto et al. (2009). Such slow wind solutions are chosen to illustrate the mechanism responsible for the formation of the $1/f$ spectrum, fast wind solutions will be considered in a forthcoming paper.

In homogeneous turbulence with equal energy in both Alfvén species the forcing controls the development of a weak (or strong) cascade, depending on whether the parallel Alfvén time is smaller (or not) than the nonlinear time. The energy density scales with perpendicular wavenumber as $k_\perp^{-2}$ or $k_\perp^{-5/3}$ (e.g., Verdini & Grappin 2012) for both species. However, in the inhomogeneous stratified open corona and solar wind, the two Alfvén wave species can in principle have very different amplitudes. We will see that they follow different cascade regimes (weak/strong) at the same time. This is the key of the results obtained in the present Letter. We show that for realistic conditions a $1/f$ magnetic spectrum forms as a consequence of the strong turbulent cascade of reflected/inward propagating waves, which reflect back (ringing) at the transition region (TR) and are advected outside the Alfvénic critical point without substantial modification, since the outward propagating waves experience a weak cascade.

2. EQUATIONS AND PARAMETERS

The model equations are obtained from the MHD equations by separating the large-scale *stationary* fields and small-scale fluctuating fields (Heinemann & Olbert 1980; Velli 1993). Among the large-scale fields, the wind speed (U) and density (ρ) are the solution of a 1D hydrodynamic solar wind model (Pinto et al. 2009; Grappin et al. 2010) with specified heating functions and assigned flux tube expansion ($A = \mathcal{F}(r)r^2$). Combining ρ with the magnetic field strength $B_\odot$ at the base of the flux tube, and requiring $BA = \text{const}$ one obtains the Alfvén speed ($V_a = B/\sqrt{4\pi\rho}$). The profiles of U, V_a, ρ, and $\mathcal{F}$ depend only on the radial distance $r = R/R_\odot$ and are plotted in the left panels of Figure 1: the bottom and top boundaries are at $r_{\rm bot} = 1.004$ and $r_{\rm top} = 19$, the Alfvénic critical point is found at $r_A \approx 17$ by choosing $B_\odot = 10\,$G. The small-scale *incompressible* velocity (u) and magnetic (b) fluctuations are orthogonal to the radial B and can be expressed through the usual Elsässer variables $z^\pm = u \mp b/\sqrt{4\pi\rho}$. We further simplify the equations by replacing the nonlinear terms and the pressure term at each position by a 2D shell model, so that the final equations read

$$\frac{\partial z_n^\pm}{\partial t} + (U \pm V_a)\frac{\partial z_n^\pm}{\partial r} - \frac{1}{4}(U \mp V_a)\left(\frac{1}{\rho}\frac{d\rho}{dr}\right) z_n^\pm + \frac{1}{4}(U \mp V_a)\left(\frac{1}{\rho}\frac{d\rho}{dr} + 2\frac{1}{A}\frac{dA}{dr}\right) z_n^\mp = T_{\rm npq}^\pm - \nu k_n^2 z^\pm, \quad (1)$$

where we take equal viscosity and resistivity (ν) and $T_{\rm npq}^\pm$ denotes the nonlinear interactions. The index n labels modes having perpendicular wavenumber $k_n = k_0 2^n$, which define the radius of concentric shells filling the (perpendicular) Fourier space. The largest transverse scale follows the flux tube expansion $k_0(r) = k_{0\odot}/\sqrt{A(r)}$, wavevectors are given by $k_\perp \equiv k_n(r) = k_0(r)2^n$, so that our Fourier space shrinks with increasing r. Two complex fields are assigned to each shell, $z_n^\pm(r,t) \equiv z^\pm(k_n, r, t)$. They have the dimension of a velocity and $|z_n^\pm|^2/2$ are the respective energies per unit mass in the shell n. We recall that nonlinear interactions are local in Fourier space, $T_{\rm npq} \propto \Sigma_{p,q} k_n z_p^\pm z_q^\mp$, with $p \sim q \sim n$ (the explicit expression and coefficients for the 2D shell model may be found in Giuliani & Carbone 1998).

Open boundaries are used at $r_{\rm bot}$ and $r_{\rm top}$. The free parameters are the input wave amplitude $z_\odot^+$, the perpendicular injection scales $k_{0\odot}$ (the forcing being imposed on $1, 2, 4k_{0\odot}$), and the correlation time of the forcing signal T_f. We choose a *strong* forcing, i.e., $T_f \simeq t_{\rm NL}^0$ by assigning: $z_\odot^+ = 10\,{\rm km\,s^{-1}}$, $k_{0\odot} = 2\pi/34{,}000\,{\rm km^{-1}}$, and $T_f = 600\,$s. With these parameters $t_{\rm NL}^0 = 1/k_0^\odot z_\odot^+ \simeq 500\,{\rm s} \simeq T_f$.

Decreasing the free parameter $B_\odot$ shifts the profile of V_a in Figure 1, to lower values, thus decreasing r_A and resizing the regions where one linear term dominates over the other linear terms (propagation, WKB, and reflection, respectively, the II, III, and IV terms on the left-hand side of Equation (1)).

Starting from the solutions $z_n^\pm(r,t)$ of Equation (1) we define frequency and wavenumber spectra. We denote by $\hat{z}_n^\pm(r, f)$ their Fourier transform with respect to time. From this we define successively the spectra $E_n^\pm(f) = E^\pm(n, f)$ and the associated reduced spectra at each radial distance r:

$$E_n^\pm(f) = |\hat{z}_n^\pm(r, f)|^2/k_\perp \quad (2)$$

$$E_f^\pm(f) = \int E_n^\pm dk_\perp \quad (3)$$

$$E_\perp^\pm(k_\perp) = \int E_n^\pm df, \quad (4)$$

where we have omitted the dependence on r. Equation (2) is the frequency spectrum of a given perpendicular mode which yields the total energy $E^\pm(r) = \sum_n |z_n^\pm|^2 = \int E_n^\pm dk_\perp df$. Equations (3) and (4) define reduced spectra, which accordingly yield $\int E_f^\pm df = \int E_\perp^\pm dk_\perp = E^\pm$ (hereafter we drop the subscripts $f, k_\perp$ when the dependence is explicit).

The correlation time $t_{\rm cor}^\pm(r, k_\perp)$ is defined as the full width half-maximum (FWHM) of the autocorrelation function AC($z^\pm$) computed at each position r, while the nonlinear time $t_{\rm NL}^\pm(r, k_\perp)$ is the time average of the eddy turnover times built from the Elsässer fields (Dobrowolny et al. 1980):

$$t_{\rm cor}^\pm(k_\perp) = {\rm FWHM}[{\rm AC}(z^\pm)_t] \quad (5)$$

$$t_{\rm NL}^\pm(k_\perp) = \langle 1/(k_\perp |z^\mp(k_\perp)|)\rangle. \quad (6)$$

Again we omitted the dependence on r, ${\rm AC}(z) = \int z(t)z(t - t')dt'$ is the autocorrelation function and $\langle\cdots\rangle$ stands for a

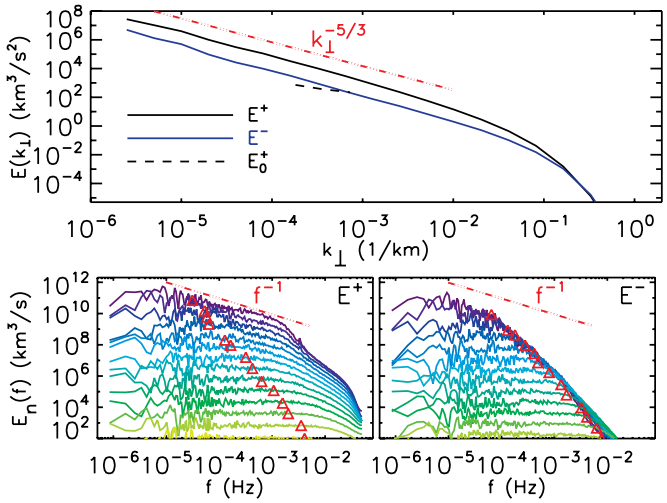

Figure 2. Top: perpendicular spectra $E^{\pm}(k_\perp)$ at $r_{\rm top}$. The input spectrum E_0^+ at $r_{\rm bot}$ is also shown (dashed line). Bottom: frequency spectra $E_n^{\pm}$ at $r_{\rm top}$ for perpendicular wavenumbers $k_0 2^n$ (with n increasing from top to bottom). Symbols mark the CB width $\Delta_{\rm CB}^{\pm}$ (see the text).

(A color version of this figure is available in the online journal.)

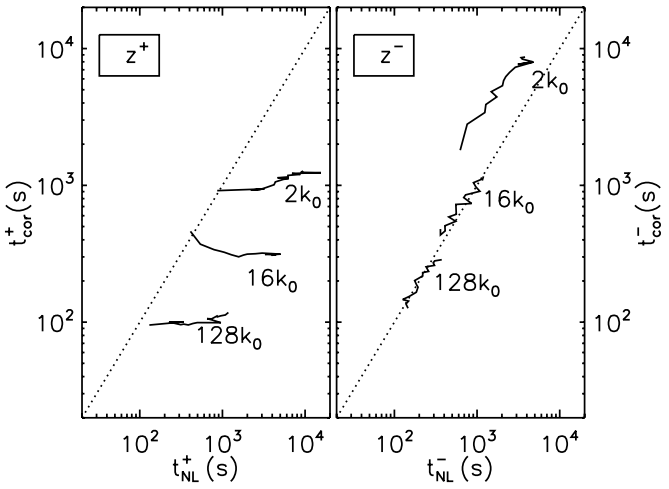

Figure 3. Correlation time $t_{\rm cor}^{\pm}$ vs. nonlinear time $t_{\rm NL}^{\pm}$ for different heliocentric distance (running from 2 $R_\odot$ to 19 $R_\odot$ from left to right on each curve) at three perpendicular wavenumbers $2k_\perp^0$, $8k_\perp^0$, $128k_\perp^0$. The dotted line is the CB condition (Equation (7)).

time average. The amplitudes of the fluctuations are computed by integrating along the perpendicular wavenumbers $z^{\pm} = \sqrt{\Sigma_n |z_n(r,t)|^2}$. The same definitions hold for u and b; the latter will be expressed in velocity units from now on (i.e., $b \to b/\sqrt{4\pi\rho}$). The equality of the two timescales defines the so-called critical balance (CB) condition:

$$t_{\rm cor}^{\pm}(k) = t_{\rm NL}^{\pm}(k), \tag{7}$$

which is supposed to hold for strong turbulence. Since the correlation time is the inverse of the width of the frequency spectrum, we can define an equivalent CB width $\Delta_{\rm CB}^{\pm} = 1/t_{\rm NL}^{\pm}$.

According to anisotropic turbulence theories (Goldreich & Sridhar 1995), this width constrains the frequency spectrum, since at a given perpendicular scale $k_\perp$ there is little energy for $f > \Delta_{\rm CB}$, while spectra are flat for $f < \Delta_{\rm CB}$.

3. RESULTS

Figure 1 shows a snapshot of the amplitude of Alfvén waves (top right) and of the kinetic and magnetic fluctuations (bottom right). In the corona $z^+ \simeq 1.5b$, $b \simeq 1.5u$. The profile of z^+ follows the wind speed profile (background dotted line) and is much larger the inward/reflected wave z^-. z^- is a smooth function of distance, while z^+ displays small-scale parallel structure, seen also in the radial profiles of u and b.

The spectral densities versus perpendicular wavenumber and frequency at $r_{\rm top} = 19$ are summarized in Figure 2. In the top panel, the time-averaged perpendicular spectra $E^{\pm}(k_\perp)$ are plotted along with the input spectrum at the base of the chromosphere (E_0^+). Both perpendicular spectra show a well-developed power law that extends about two decades with a slope $-5/3$. The ratio $E_\perp^+/E_\perp^-$ is about constant in the inertial range. The input perpendicular spectrum E_0^+ (dashed line) appears in the middle of the inertial range of the spectra at $r_{\rm top}$, as the flux tube expansion has strongly expanded the perpendicular scales between the surface and $r_{\rm top}$ (by a factor of 100).

In the bottom panels of Figure 2 the frequency spectra, $E_n^{\pm}(f)$, are plotted for each perpendicular mode n. Symbols mark the equivalent CB width $\Delta_{\rm CB}^{\pm}$. The E^- spectra (right) are very well bounded by the CB condition, falling off sharply in the weak turbulence range ($f > \Delta_{\rm CB}^-$), and having flat spectra in the strong turbulence range ($f < \Delta_{\rm CB}^-$), with few exceptions for large-scale eddies ($n = 0, 1, 2$). On the contrary, E_n^+ has a substantial overexcitation of high frequencies at large perpendicular scales and in the whole weak range, which reflects the fine-scale (parallel) spatial structure of z^+ seen in Figure 1. This overexcitation has an approximate slope $1/f$ and extends from the CB boundary to about $1/T_f \simeq 2 \times 10^{-3}$ Hz.

The slope of the frequency spectrum has been found to depend on turbulence forcing strength $T_f/t_{\rm NL}^0$ in homogenous *shell* RMHD simulations (Verdini & Grappin 2012) and to extend beyond forced scales. The situation is different here because we cannot really control the forcing turbulence strength: the nonlinear time for z^+ depends on the reflected amplitude z^-, an output of the simulation. An a posteriori estimate yields a turbulence strength $t_{\rm cor}^+/t_{\rm NL}^+ < 1$ so that z^+ is indirectly forced in the weak regime. Coming back to the strong turbulence range, one can see that large eddies have an approximate slope of $1/f$ in both E^- and E^+: these low-frequency fluctuations are *linearly* coupled by density gradients (reflection) that force the spectra to resemble each other.

The turbulence regime at different heliocentric distances can be identified in Figure 3, where we plot the correlation time versus the nonlinear time for three wavenumbers ($2k_0$, $8k_0$, $128k_0$) at heliocentric distances, running from left ($r = 2$) to right ($r = 19$) along the solid lines. The CB condition (Equation (7)) is drawn as a dotted line and separates the strong and weak regimes (above and below, respectively). The reflected wave z^- is always in a strong turbulence regime and follows the CB condition at any position, except for a small offset at low wavenumbers due to the linear coupling (reflection) at large scale. On the contrary the correlation time of z^+ is almost horizontal, i.e., almost independent of the nonlinear time and of distance, and lies entirely in the weak turbulence regime. Since $t_{\rm cor}$ is the inverse of the width of the frequency spectrum, one can conclude that the E^+ spectrum does not change much as it propagates outward, only becoming a bit narrower at large scales. Instead, the E^- spectrum widens while propagating backward from r_A, according to CB. Once it arrives at the TR it experiences strong reflection and feeds the E^+ spectrum; this can be argued by

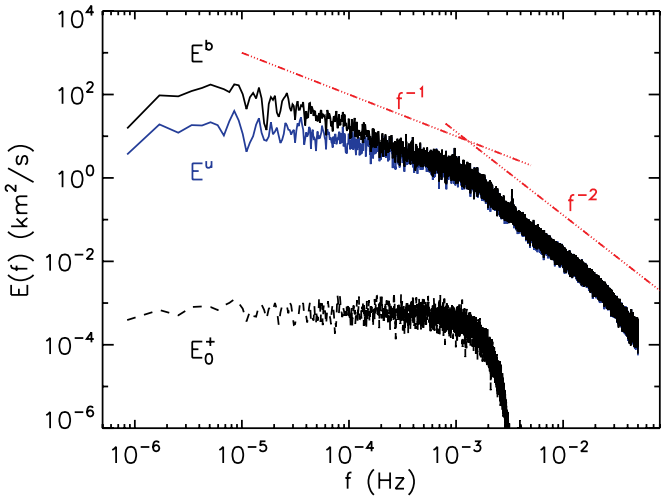

Figure 4. Reduced frequency spectra for $E^{u,b}$ at $r_{\rm top}$ (solid gray and black line, respectively) and input spectrum E_0^+ at $r_{\rm bot}$ (dashed line).

(A color version of this figure is available in the online journal.)

noting that $t^+_{\rm cor} \lesssim t^-_{\rm cor}$ at $r = 2$ (the low end of the curves). At larger distances $t^+_{\rm cor} \ll t^-_{\rm cor}$, showing that E^+_n is wider than E^-_n in the whole corona, the difference owing to its high-frequency overexcitation.

The $1/f$ spectrum appearing at large perpendicular scales in E^+ is thus made up of two parts, each occupying about one decade from $f \simeq 10^{-5}$ Hz, which originate from two different mechanisms: linear coupling with E^- at low frequencies (the strong turbulence range) and weak turbulent cascade at intermediate frequencies. This is summarized in Figure 4 where the reduced frequency spectra $E^{u,b}(f)$ of kinetic and magnetic energy at $r = r_{\rm top}$ are shown (along with the input spectrum at the base of the chromosphere E^+_0). The spectrum of E^b shows the $1/f$ slope inherited from the large-scale eddies in E^+, in which one can recognize the above two components, and a break appears at about $f \simeq 10^{-3}$ Hz where the slope switches to -2. The break coincides with the width of the forcing spectrum ($1/T_f \simeq 2 \times 10^{-3}$ Hz) and the -2 slope is consistent with the fall-off at high frequencies in $E^b_n \simeq E^+_n$. Note that linear propagation alone would lead to a magnetic spectrum with slope $f^{-1/2}$ (not shown), thus nonlinear interactions are fundamental to obtain the $1/f$ slope. The spectrum of E^u is practically identical to E^b for $f \gtrsim 10^{-4}$ Hz due to the same overexcitation in the weak regime. For lower frequencies instead the slope of E^u is flatter, having a value of about $-1/2$.

4. DISCUSSION

Why the $1/f$ extends down to low frequencies only in E^b can be understood by examining the wave reflection at the TR, where density gradients are higher. For frequencies $f \lesssim \max[|dV_a/dr|] \simeq 2$ Hz, one can write $z^- = -(1-\epsilon)z^+$, where $\epsilon = V_a^{\rm chrom}/V_a^{\rm cor} \ll 1$ is the Alfvén speed contrast between the chromosphere and corona (Hollweg 1984; van Ballegooijen et al. 2011; Verdini et al. 2012). At the TR, $b \simeq z^\pm$ and $u \ll z^\pm$, thus reflection transfers the low-frequency large-eddy spectrum of E^- to E^b but not to E^u. In reality reflection occurs in the whole low corona (for $r \lesssim 3\,R_\odot$ at frequencies $f < 5 \times 10^{-3}$ Hz) and is a continuous process. Moreover, reflected waves are made of two components: a classical one, propagating backward in the region $U < V_a$ and subject to ringing in the low corona, and an anomalous component that instead propagates outward with the mother wave (Velli et al. 1989; Hollweg & Isenberg 2007; Verdini et al. 2009). Nonlinear interactions are not limited to the duration of the encounter of colliding $z^\pm$ wavepackets, but part of them occur on the common outward propagation path. This is why linear and also nonlinear couplings affect the low tail of the $1/f$ spectrum.

Bearing in mind that z^- is entirely generated by reflection inside the solar atmosphere, we examine now what happens if we increase the input turbulence strength (i.e., the control parameter $T_f/t^0_{\rm NL}$) by either increasing the correlation time T_f or decreasing the input nonlinear time $t^0_{\rm NL} = 1/k_{0\odot}z^+_\odot$. By imposing a shorter input nonlinear time, no matter if through $z^+_\odot$ or $k_{0\odot}$, we increase the strength of the cascade for z^-. The strength of the z^+ cascade will increase only slightly, since the reflected wave will be damped more strongly, yielding approximately the same $t^+_{\rm NL}$. The spectrum of E^+ will thus be affected only slightly, except that now nonlinear coupling will dominate over reflection in the low corona, eroding the very low frequency tail of the $1/f$ spectrum in E^b. If instead we choose a longer correlation time at input, we increase the amount of reflected waves thus also increasing the strength of the cascade for z^+. This time the high-frequency tail of the $1/f$ spectrum will be eroded, since a stronger cascade reduces the energy in the overexcited weak-turbulence regime of E^+. Finally, one can vary the importance of linear/nonlinear coupling through the other free parameter $B_\odot$. Taking a smaller chromospheric magnetic field will lower the Alfvénic critical point, reducing the importance of linear terms compared to the nonlinear ones in Equation (1). The changes in the E^b spectrum are similar to those discussed above for a shorter $t^0_{\rm NL}$. Note however that halving $B_\odot$ moves r_A to a distance of 8 $R_\odot$, so that one is limited to small variations of this parameter. A last remark concerns the non-local couplings in the Fourier space that are neglected in the shell model employed in this work. In principle, they could change the perpendicular spectra and the strength of the cascade. However, our understanding of the process of formation of the $1/f$ spectrum is that it comes from the different nature of the two direct z^- and z^+ cascades, not because of an inverse cascade as in the dynamo process. We expect these direct cascades not to change when including nonlocal interactions.

The formation of the $1/f$ spectrum by nonlinear and linear coupling in the sub-Alfvénic solar wind appears to be quite solid, however its relation to the interplanetary spectrum observed at 0.3 AU is not straightforward. Beyond r_A the solar wind expansion causes the rotation of the magnetic field, a slower production of reflected waves, and a decrease of wave numbers perpendicular to the radial direction (Grappin et al. 1993). The latter two actually suggest a freezing of the spectra. On the contrary, the magnetic field rotation causes instabilities and wave coupling/decay that could modify the spectrum. Numerical simulations of MHD equations in 1D and 2D incorporating the effect of an expanding solar wind (Grappin et al. 1993; Grappin & Velli 1996) suggest that the decay and instability rates are delayed with respect to the non-expanding case, so that a freezing of the advected spectra may be a good approximation, at least until 0.3 AU. If one assumes no further evolution, the double power law measured by *Helios* at 0.3 AU, may result from the combination of the parallel and perpendicular reduced spectra. At low frequency the parallel spectrum dominates with its characteristic slope -1, while at higher frequencies its steep spectral slope (-2) is masked by the more energetic perpendicular spectrum (with a $-5/3$ slope).

Our theory might well be tested by the measurements of Solar Probe Plus.

We thank E. Buchlin for useful suggestions while implementing the background solar wind in the numerical code. A.V. acknowledges support from the Belgian Federal Science Policy Office through the ESA-PRODEX program. The research described in this paper was carried out in part at the Jet Propulsion Laboratory, California Institute of Technology, under a contract with the National Aeronautics and Space Administration.

REFERENCES

Bavassano, B., Dobrowolny, M., Mariani, F., & Ness, N. F. 1982, J. Geophys. Res., 87, 3617
Bruno, R., & Carbone, V. 2005, Living Rev. Sol. Phys., 2, 4
Close, R. M., Parnell, C. E., Longcope, D. W., & Priest, E. R. 2004, ApJ, 612, L81
Denskat, K. U., & Neubauer, F. M. 1983, in NASA Conference Publication, Vol. 228, Observations of Hydromagnetic Turbulence in the Solar, ed. M. Neugebauer (NASA CP-2280; Washington, DC: NASA), 81
Dmitruk, P., & Matthaeus, W. H. 2007, Phys. Rev. E, 76, 1
Dmitruk, P., Mininni, P. D., Pouquet, A., Servidio, S., & Matthaeus, W. H. 2011, Phys. Rev. E, 83, 66318
Dobrowolny, M., Mangeney, A., & Veltri, P. 1980, Phys. Rev. Lett., 45, 144
Giuliani, P., & Carbone, V. 1998, Europhys. Lett., 43, 527
Goldreich, P., & Sridhar, S. 1995, ApJ, 438, 763
Grappin, R., Léorat, J., Leygnac, S., & Pinto, R. 2010, in AIP Conf. Proc. 1216, 12th Int. Solar Wind Conference, ed. M. Maksimovic et al. (Melville, NY: AIP), 24
Grappin, R., & Velli, M. 1996, J. Geophys. Res., 101, 425
Grappin, R., Velli, M., & Mangeney, A. 1993, Phys. Rev. Lett., 70, 2190
Heinemann, M., & Olbert, S. 1980, J. Geophys. Res., 85, 1311
Hollweg, J. V. 1984, Sol. Phys., 91, 269
Hollweg, J. V., & Isenberg, P. A. 2007, J. Geophys. Res., 112, 1
Marsch, E., & Tu, C.-Y. 1990, J. Geophys. Res., 95, 11945
Matthaeus, W. H., Breech, B., Dmitruk, P., et al. 2007, ApJ, 657, L121
Matthaeus, W. H., & Goldstein, M. L. 1986, Phys. Rev. Lett., 57, 495
Pinto, R., Grappin, R., Wang, Y.-M., & Léorat, J. 2009, A&A, 497, 537
Roberts, D. A. 1992, in Solar Wind Seven Colloquium, ed. E. Marsch & R. Schwenn (Oxford: Pergamon Press), 533
Tu, C.-Y., Pu, Z.-Y., & Wei, F.-S. 1984, J. Geophys. Res., 89, 9695
van Ballegooijen, A. A., Asgari-Targhi, M., Cranmer, S. R., & DeLuca, E. E. 2011, ApJ, 736, 3
Velli, M. 1993, A&A, 270, 304
Velli, M., Grappin, R., & Mangeney, A. 1989, Phys. Rev. Lett., 63, 1807
Verdini, A., & Grappin, R. 2012, Phys. Rev. Lett., submitted (arXiv:1204.2094)
Verdini, A., Grappin, R., & Velli, M. 2012, A&A, 538, A70
Verdini, A., Velli, M., & Buchlin, E. 2009, ApJ, 700, L39